Article

The timing of decreasing coastal flood protection due to sea-level rise

Check for updates

Tim H. J. Hermans [1,2,3] ✉, Víctor Malagón-Santos [1], Caroline A. Katsman [4], Robert A. Jane [5], D. J. Rasmussen [6], Marjolijn Haasnoot [7,8], Gregory G. Garner [9], Robert E. Kopp [10,11], Michael Oppenheimer [6,12,13] & Aimée B. A. Slangen [1]

Sea-level rise amplifies the frequency of extreme sea levels by raising their baseline height. Amplifications are often projected for arbitrary future years and benchmark frequencies. Consequently, such projections do not indicate when flood risk thresholds may be crossed given the current degree of local coastal protection. To better support adaptation planning and comparative vulnerability analyses, we project the timing of the frequency amplification of extreme sea levels relative to estimated local flood protection standards, using sea-level rise projections of IPCC AR6 until 2150. Our central estimates indicate that those degrees of protection will be exceeded ten times as frequently within the next 30 years (the lead time that large adaptation measures may take) at 26% and 32% of the tide gauges considered, and annually at 4% and 8%, for a low- and high-emissions scenario, respectively. Adaptation planners may use our framework to assess the available lead time and useful lifetime of protective infrastructure.

Extreme sea levels due to tides, storm surges and waves can lead to coastal flooding and cause severe damage to people, infrastructure and the environment[1]. Due to climate change, the return frequency of extreme sea levels is projected to increase in many regions around the world, leading to higher coastal flood risk[2]. The main driver of these increases is relative sea-level rise (SLR)[2–4], which raises the baseline height of extreme sea levels. Assuming a stationary extremes distribution, projections of the return frequency increase of extreme sea levels due to SLR can be made by combining observation- or model-based inferences of the historical extremes distribution with projected SLR, for instance, for radiative forcing scenarios[1,5–11] or global warming levels[12,13]. The projected probability increase of a certain extreme sea level is often presented as an amplification factor (AF) that indicates the ratio between the future and historical probability of that extreme sea level.

AFs are often projected for an arbitrary future year (for example, 2100) and referenced to a single historical extreme event, regardless of location[14]. Typically the extreme sea level with a probability of 0.01 yr^{-1} (that is, a return frequency of 1 in 100 years) is chosen as a benchmark (for example, refs. [1,9,11,13]). Such projections are of limited salience because local coastal flood protection may be designed to withstand extreme sea levels with a probability different from 0.01 yr^{-1} and a large amplification of the historical 0.01 yr^{-1} extreme (denoted $AF_{0.01}$) does not necessarily cause a large change in impact[14]. Moreover, such projections do not convey when certain flood risk thresholds may be crossed nor the uncertainty in that timing, which is crucial

[1]Department of Estuarine and Delta Systems, NIOZ Royal Netherlands Institute for Sea Research, Yerseke, the Netherlands. [2]Department of Geosciences and Remote Sensing, Delft University of Technology, Delft, the Netherlands. [3]Institute for Marine and Atmospheric Research Utrecht, Utrecht University, Utrecht, the Netherlands. [4]Department of Hydraulic Engineering, Delft University of Technology, Delft, the Netherlands. [5]Department of Civil, Construction and Environmental Engineering, University of Central Florida, Orlando, FL, USA. [6]Princeton School of Public and International Affairs, Princeton University, Princeton, NJ, USA. [7]Deltares, Delft, the Netherlands. [8]Department of Geosciences, Utrecht University, Utrecht, the Netherlands. [9]GRO Intelligence, New York, NY, USA. [10]Department of Earth and Planetary Sciences, Rutgers University, Piscataway, NJ, USA. [11]Rutgers Institute of Earth, Ocean, and Atmospheric Sciences, Rutgers University, New Brunswick, NJ, USA. [12]Department of Geosciences, Princeton University, Princeton, NJ, USA. [13]High Meadows Institute, Princeton University, Princeton, NJ, USA. ✉e-mail: t.h.j.hermans@uu.nl

for planning when and how to adapt[14–18]. A few studies have included timing information, but they only communicated the first decade in which the probability of the 0.01 yr⁻¹ extreme sea level will have increased to >1 yr⁻¹ (AF$_{0.01}$ > 100)[1,13] or when its probability will double (AF$_{0.01}$ = 2)[19], are limited to the United States[10,20] or focus on changes in population exposure[14,16].

Here, we introduce a framework to project the timing of AFs and its uncertainty, relating the AFs to return frequencies corresponding to estimated local flood protection standards[21] instead of to an arbitrary historical return frequency. Our projections therefore indicate the timing of different decreases in the degree of local coastal protection (Fig. 1), some of which may occur before large adaptation measures, which may have lead times of up to ~30 years[15,18,22], can be completed. As such, our framework can be used to assess the time left for adaptation under different emissions scenarios and support the planning of new adaptation measures, given cost–benefit considerations and the required lead time and envisioned lifetime of different adaptation measures[23–25]. For our projections, we use the relative SLR projections of the IPCC AR6 up to 2150[11,26] for a range of Shared Socioeconomic Pathway (SSP) scenarios[27]. To infer the historical extreme sea-level distributions, we apply a peak-over-threshold method with an automatic threshold selection[28] and fit generalized Pareto distributions to the daily maxima in tide gauge observations from Global Extreme Sea Level Analysis v.3.0 (GESLA3)[29,30] (Methods).

Required SLR

To compute the timing of different frequency amplifications of a reference return frequency f_{Ref} we first compute the SLR required for them (Methods). The required SLR refers to how much the historical return curve, which relates the return height of extreme sea levels to their return frequency, needs to be shifted up to establish a given amplification of f_{Ref} (illustrated in Fig. 2a). For example, with the return curve in Fig. 2a a reference return frequency of 0.05 yr⁻¹ (that is, once every 20 years) would require 0.6 m of SLR to be amplified by a factor of 100 (to 5 yr⁻¹). While typically f_{Ref} is set to 0.01 yr⁻¹, we base f_{Ref} on estimates of local flood protection standards (FLOPROS) ($f_{Ref} = f_{FLOPROS}$; Fig. 2b), which were produced using the FLOPROS modelling approach based on the gross domestic product per capita and absolute risk at subnational scales[21,31]. These estimates are used here as the current degree of coastal protection because systematic empirical evidence is lacking[32].

The SLR required for amplifications of $f_{FLOPROS}$ by factors 10 and 100 (denoted AF$_{FLOPROS}$ = 10 and 100), or equivalently, for 10- and 100-fold decreases in the estimated degree of protection, varies locally (Fig. 3a,b, central estimates). This is primarily governed by the forms of the return curves, which depend on the parameters of the generalized Pareto distribution (Extended Data Fig. 1). For other AFs, see the Data Availability. The required SLR for AF$_{FLOPROS}$ = 10 and 100 ranges from one to a few tens of centimeters at many tide gauges along the eastern tropical Pacific coast, in southern Europe, South Africa, Southeast Asia and eastern Australia (Fig. 3a,b), implying that at these locations SLR will reduce the degree of protection relatively fast. This likely also holds for many small islands in the Pacific Ocean[1], which were not included because no FLOPROS estimates were available (Methods). The required SLR is larger at tide gauges in the Gulf of Mexico, along the east coast of the United States and in the North Sea (Fig. 3a,b). Broadly agreeing with previous characterizations[10,19,33], the required SLR is larger at locations that experience a larger variability of extremes (for example, due to strong tropical, extratropical storms and/or tides) and therefore have a relatively steep return curve, and vice versa. The required SLR for AF$_{FLOPROS}$ = 10 (Fig. 3a) is, on average, 25 cm smaller than for AF$_{FLOPROS}$ = 100 (Fig. 3b).

The required SLR is also influenced by the estimated degree of protection (Fig. 2b), which controls which part of the return curve is evaluated. For instance, at a particular location the 0.001 yr⁻¹ and 0.1 yr⁻¹ probability events could differ in height less than the 0.01 yr⁻¹ and 1 yr⁻¹
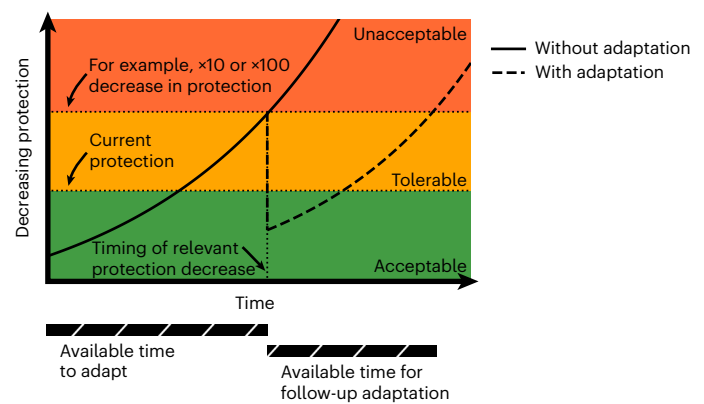

Fig. 1 | Timing of the decreasing degree of protection with and without adaptation. Our framework projects the timing of different decreases in the degree of local coastal protection due to SLR and can be used to assess the available adaptation time.

probability events. Hence, perhaps counterintuitively, a higher degree of protection does not necessarily mean that more SLR is required for the same decrease in protection. This is shown schematically in Extended Data Fig. 2 and explains why the SLR required for the same amplification of $f_{FLOPROS}$ and 0.01 yr⁻¹ differ (Extended Data Fig. 3). For example, less SLR is required for AF$_{FLOPROS}$ = 100 than for AF$_{0.01}$ = 100 at the Dutch and US Gulf coasts, because the estimated degree of protection is associated with a probability lower than 0.01 yr⁻¹ and the slope of the return curve decreases as the probability decreases at the Dutch coast, and vice versa at the US Gulf coast. These differences add to the importance of choosing locally meaningful benchmark frequencies for AFs, as argued in ref. [14] and implemented here.

The uncertainties in the distribution parameters (Methods) cause uncertainty in the required SLR (Fig. 3c,d). Evaluated across locations, the median 5–95% range is approximately 17 cm wide for AF$_{FLOPROS}$ = 10 (Fig. 3c) and 22 cm wide for AF$_{FLOPROS}$ = 100 (Fig. 3d). The uncertainty tends to be large at locations that experience large variability and/or have a relatively short record length. Specifically in tropical cyclone regions, such as the US east coast and the subtropical coast of Asia, uncertainties are large because tropical cyclones are often undersampled in tide gauge records[34–36]. The uncertainty is also relatively large at locations with a high (estimated) degree of protection (for example, in the Netherlands and at Long Island (United States); Fig. 2b), where evaluating the required SLR requires a large degree of extrapolation of the observational records. Synthetic data approaches[35,37] could help reduce these uncertainties. The uncertainty in the required SLR shows when aggregating our estimates globally: considering the central estimate at each tide gauge, the fractions of tide gauges at which AF$_{FLOPROS}$ = 10 and AF$_{FLOPROS}$ = 100 require 0.5 m of SLR or less are 89% and 61%, respectively (Fig. 3e,f, right), but those fractions increase or decrease when considering, for instance, the 5th or 95th percentile at each tide gauge (Fig. 3e,f, left).

Projected timing

Next, we project the timing of different AF$_{FLOPROS}$ by combining required SLR with projected SLR (Methods). Results for AF$_{FLOPROS}$ = 10 and 100 (that is, 10- and 100-fold decreases in the estimated degrees of protection) are shown for a low-emissions (SSP1-2.6) and high-emissions (SSP3-7.0) scenario in Fig. 4, and for other emissions scenarios in Extended Data Fig. 4. For other AFs, see the Data availability. Our central estimates indicate that under SSP1-2.6, AF$_{FLOPROS}$ = 10 and 100 will occur before 2150 at the majority of the 474 tide gauges (Fig. 4a,b). At a smaller fraction of tide gauges (26% and 2%, respectively), these amplifications will occur within the next 30 years (Fig. 4c,d). The timing is earliest at locations with substantial projected SLR (Extended Data
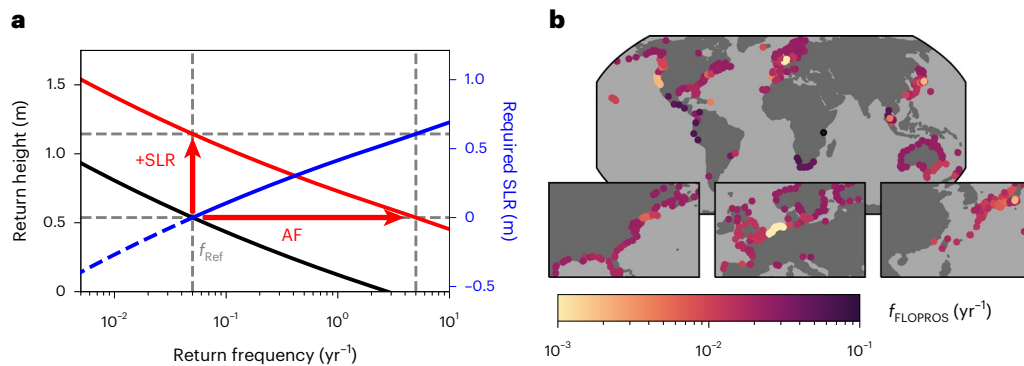
Fig. 2 | Required SLR and FLOPROS estimates. a, Schematic illustration of the required SLR (blue) for the amplification of reference return frequency f_{Ref}, derived from a historical return curve (black, shifted up to red due to SLR).

b, Estimates of flood protection standards[21] interpolated to GESLA3 tide gauges ($f_{FLOPROS}$) (yr^{-1}), used for f_{Ref}. The map insets in **b** zoom in on three regions densely covered with tide gauges (US East Coast, Europe and Southeast Asia).
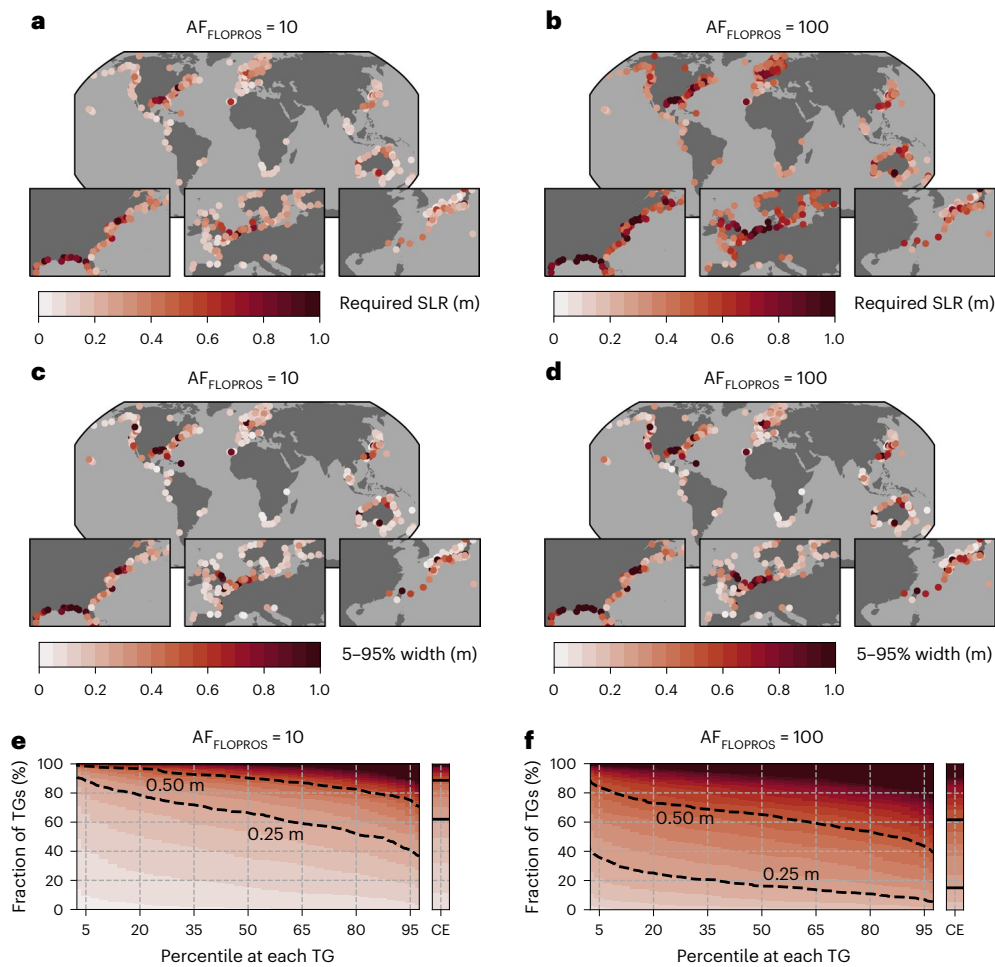
Fig. 3 | Required SLR for AF$_{FLOPROS}$ = 10 and 100. a,b, Central estimate of required SLR (m) for AF$_{FLOPROS}$ = 10 (**a**) and 100 (**b**) at GESLA3 tide gauges. **c,d,** Width of the 5–95% range of required SLR (m) for AF$_{FLOPROS}$ = 10 (**c**) and 100 (**d**). **e,f,** Fraction of tide gauges (TGs) requiring the displayed amount of SLR (m) or less for AF$_{FLOPROS}$ = 10 (**e**) and 100 (**f**), for different percentiles at each TG (left) and

for the central estimate (CE, right). The contours in **e** and **f** denote required SLR of 0.25 m and 0.50 m, both for the percentiles and the CE. The map insets in **a**, **b**, **c** and **d** zoom in on three regions densely covered with tide gauges (US East Coast, Europe and Southeast Asia).

Fig. 5) and small required SLR (Fig. 3), for instance, along the eastern Pacific coastline and in southern Europe. The amplifications are not projected to occur before 2150 at locations with larger required than projected SLR (white circles) or with a projected relative sea-level fall (cyan diamonds) (Fig. 4a,b,e,f).

Importantly, our framework allows us to express the uncertainty of AFs at each location in terms of timing rather than magnitude (see Fig. 4c,d,g,h and maps of the 5th and 95th percentiles in Extended Data Fig. 6). The timing uncertainty of the amplifications under SSP1-2.6 is large: 90% and 62% of the locations have at least a 5% probability
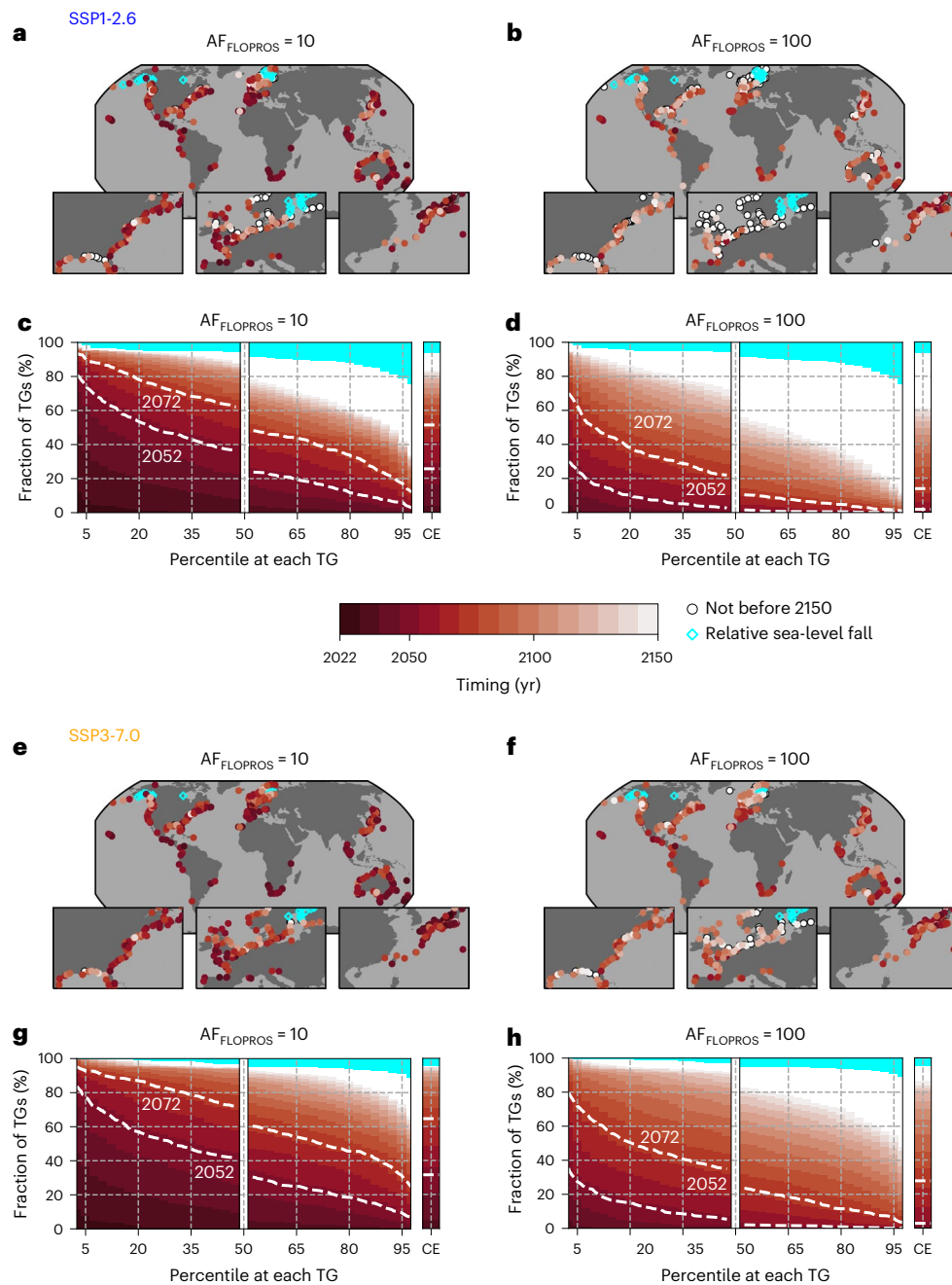
Fig. 4 | Projected timing of AF$_{FLOPROS}$ = 10 and 100. a,b, Central estimate of the timing (yr) of AF$_{FLOPROS}$ = 10 (**a**) and 100 (**b**) at GESLA3 tide gauges (SSP1-2.6). **c,d,** Fraction of tide gauges (TGs) for which AF$_{FLOPROS}$ = 10 (**c**) and 100 (**d**) are projected to occur in or before the displayed year, for different percentiles of the probability box at each TG (left), and for the central estimate (CE, right) (SSP1-2.6). **e,f,** Central estimate of the timing (yr) of AF$_{FLOPROS}$ = 10 (**e**) and 100 (**f**) at GESLA3 tide gauges (SSP3-7.0). **g,h,** Fraction of tide gauges (TGs) for which AF$_{FLOPROS}$ = 10 (**g**) and 100 (**h**) are projected to occur in or before the displayed
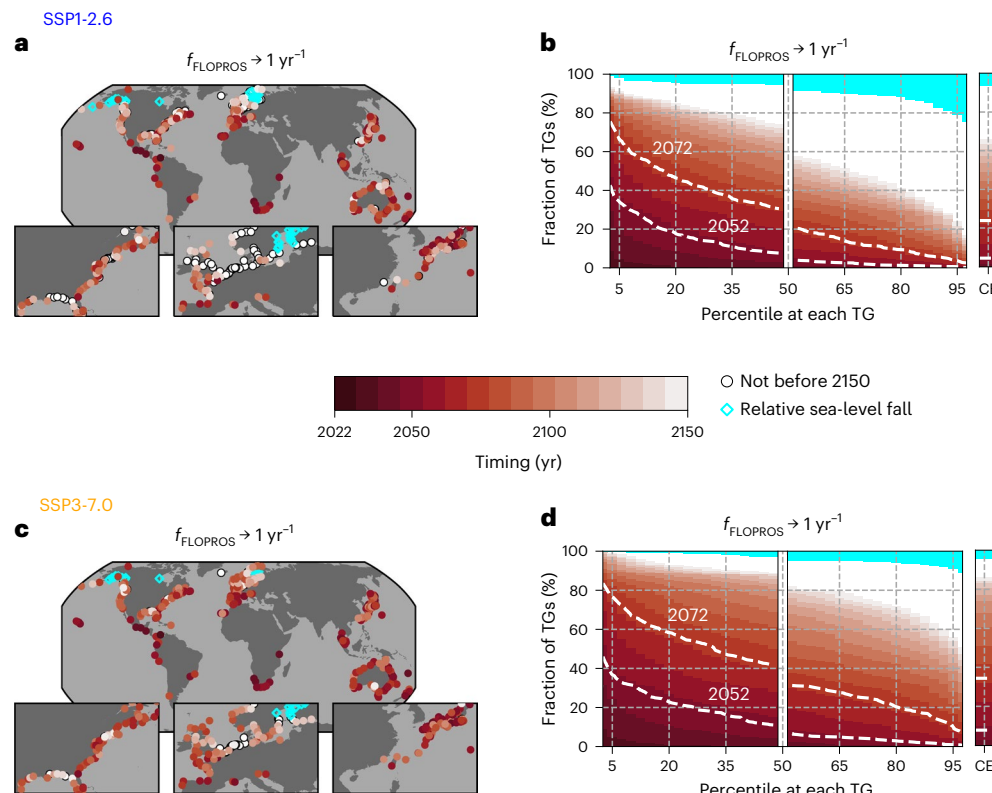
year, for different percentiles of the probability box at each TG (left), and for the central estimate (CE, right) (SSP3-7.0). White indicates where the projected timing evaluates to later than 2150 and cyan indicates where a relative sea-level fall is projected. The white dashed contours in **c**, **d**, **g** and **h** denote a projected timing within 30 and 50 years from now (2052 and 2072, respectively), both for the percentiles and the CE. The map insets in **a**, **b**, **e** and **f** zoom in on three regions densely covered with tide gauges (US East Coast, Europe and Southeast Asia).

of AF$_{FLOPROS}$ = 10 and 100, respectively, occurring within the next 50 years, while only 42% and 17%, respectively, have a 95% probability of those AFs occurring before 2150 (Fig. 4c,d). As these fractions are based on the probability boxes bounding the distributions for different sea-level projection workflows at each tide gauge (Methods), Fig. 4c,d are discontinuous across the median. The uncertainty in the projected timing results from both the uncertainty in the sea-level projections and the uncertainty in the distribution parameters. Hence, while an

amplification may occur earlier than the central estimate indicates, that earlier timing could be caused not only by a larger projected SLR but also by a smaller required SLR. Consequently, while the associated decrease in protection may occur earlier, counteracting it would also require a smaller protection height increment.

The projected timing of decreases in the estimated degrees of protection is considerably earlier under SSP3-7.0: our central estimates (Fig. 4e,f) indicate that AF$_{FLOPROS}$ = 10 and 100 are projected to occur

Fig. 5 | Projected timing until annual exceedance of estimated protection standards. a, Central estimate of the timing (yr) of the amplification of $f_{FLOPROS}$ to 1 yr^{-1} at GESLA3 tide gauges (SSP1-2.6). **b**, Fraction of tide gauges (TGs) for which $f_{FLOPROS}$ is projected to amplify to 1 yr^{-1} in or before the displayed year, for different percentiles of the probability box at each TG (left) and for the central estimate (CE, right) (SSP1-2.6). **c**, Central estimate of the timing (yr) of the amplification of $f_{FLOPROS}$ to 1 yr^{-1} at GESLA3 tide gauges (SSP3-7.0). **d**, Fraction of tide gauges (TGs) for which $f_{FLOPROS}$ is projected to amplify to 1 yr^{-1} in or before the displayed year, for different percentiles of the probability box at each TG (left) and for the central estimate (CE, right) (SSP3-7.0). White indicates where the projected timing evaluates to later than 2150 and cyan indicates where a relative sea-level fall is projected. The white dashed contours in **b** and **d** denote a projected timing within 30 and 50 years from now (2052 and 2072, respectively), both for the percentiles and the CE. The map insets in **a** and **c** zoom in on three regions densely covered with tide gauges (US East Coast, Europe and Southeast Asia).

within the next 50 years at 65% and 28% of all tide gauges, respectively, and within the next 30 years at 32% and 3% of all tide gauges (Fig. 4g,h), respectively. Almost all tide gauges have at least a 5% probability of AF$_{FLOPROS}$ = 100 occurring before 2150, even those in regions experiencing large land uplift (Extended Data Fig. 6f). Approximately 77% and 27% of the tide gauges have at least a 5% probability of AF$_{FLOPROS}$ = 10 and 100 occurring within the next 30 years (Fig. 4g,h), respectively. The fraction of tide gauges reported here at which an AF of 100 is met before a given year differs from recent IPCC estimates[1,11] due to methodological differences (for example, Extended Data Fig. 7).

With our framework, it is also possible to project when the estimated current degree of coastal protection will no longer be sufficient to protect against a sea level occurring on average once a year. This may inform local decision makers of the urgency of starting adaptation planning. Our central estimates (Fig. 5a,c) indicate that this may occur before 2150 at 66% and 86% of all tide gauges, within 50 years at 24% and 34% of all tide gauges, and within 30 years at 4% and 8% of all tide gauges, under SSP1-2.6 and SSP3-7.0, respectively, and potentially sooner for lower probabilities (Fig. 5b,d).
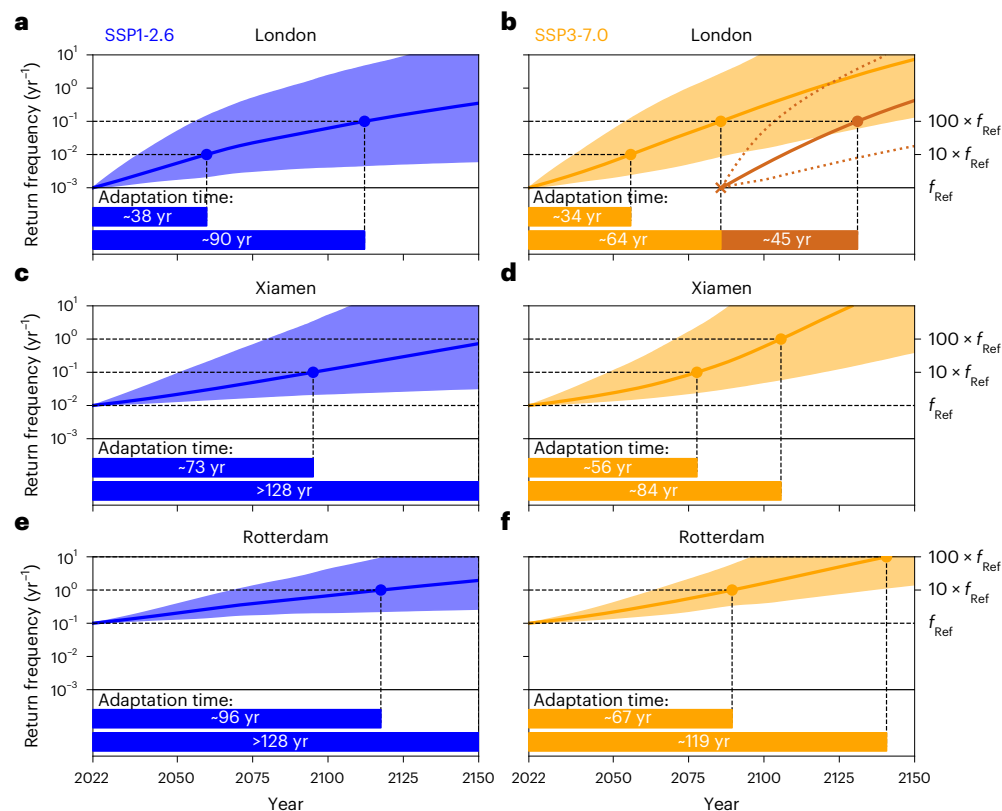
Using the projected timing

To illustrate how our projection framework could aid adaptation planning, we show examples for the tide gauges nearest to London (United Kingdom), Xiamen (China) and Rotterdam (the Netherlands). For London, we set f_{Ref} to 0.001 yr^{-1} according to the design standard of the Thames Barrier[38]; for Xiamen, we use f_{Ref} = 0.01 yr^{-1} (ref. [39]); and for Rotterdam, we set f_{Ref} = 0.10 yr^{-1}, which approximates the design closure

frequency of the Maeslant storm surge barrier[40]. These examples are mainly illustrative, as they are based on a single degree of protection and tide gauge record, while the local degree of protection, the flooding hazard and the impact of flooding may vary within a city and differ from that at the tide gauge.

The amplification of the frequencies chosen is projected to occur fastest in London and slowest in Rotterdam (Fig. 6), governed by their projected and required SLR (Extended Data Fig. 8). The uncertainty also varies by location (shading), but is larger under SSP1-2.6 than under SSP3-7.0 at all three locations because the timing is later under SSP1-2.6. The constraints on the available adaptation time that these projections pose depend on which decreases in the degree of protection or increases in barrier closure frequency are unacceptable (Fig. 1). If a factor 10 would be unacceptable, our central estimates (Fig. 6, solid lines) indicate that adaptation would be required in London, Xiamen and Rotterdam within the next 38, 73 and 96 years, respectively, under SSP1-2.6 and within the next 34, 56 and 67 years, respectively, under SSP3-7.0. If a factor 100 would be unacceptable, the available adaptation time would be decades longer (Fig. 6). For Rotterdam, an amplification of factor 10 or higher may indeed incentivize adaptation (for example, replacement) because annual or more frequent closures of the storm surge barrier are anticipated to be problematic for ecology and navigation[15].

Decreasing adaptation time

While Fig. 6 shows the projected timing of decreases in the degree of protection from 2022, the rate of SLR is projected to change in the

Fig. 6 | Projected timing in three coastal cities. a–e, Projected timing (yr) of the amplification of locally salient benchmark return frequencies in London (f_{Ref} = 0.001 yr⁻¹, tide gauge 'Sheerness') (**a,b**), Xiamen (f_{Ref} = 0.01 yr⁻¹, tide gauge 'Xiamen') (**c,d**) and Rotterdam (f_{Ref} = 0.10 yr⁻¹, tide gauge 'Hoek van Holland') (**e,f**), under SSP1-2.6 (blue) (**a,c,e**) and SSP3-7.0 (orange) (**b,d,f**), respectively.

The coloured lines indicate the central estimates and the shading the 5–95% ranges of the probability boxes. The bars at the bottom indicate the central estimates of the time available to adapt to 10- and 100-fold example amplifications of f_{Ref}. In **b**, dark orange indicates the projected timing taking 2086 instead of 2022 as a starting year.

future, which will affect the available adaptation time[18]. Suppose adaptation measures are taken in London before the degree of protection will have decreased 100-fold in 64 years from now (under SSP3-7.0, Fig. 6b), such that the degree of protection will have been restored to 0.001 yr⁻¹ in 2086. After that, it will only take 45 instead of 64 years for the degree of protection to decrease 100-fold again (Fig. 6b, dark orange) because SLR is projected to accelerate under SSP3-7.0, leaving increasingly less time for adaptation. This effect is scenario dependent, as under SSP1-2.6, for instance, the rate of SLR is projected to level off.

Discussion

In this study, we have introduced a framework that extends the emerging timing perspective on SLR[11,15,17,18] to the frequency amplification of extreme sea levels. Moreover, by relating the AFs to estimated local flood protection standards, our framework can be used to project the timing of different decreases in the local degree of protection (Fig. 1). This is useful because the timing of unacceptable decreases in the degree of protection, and therefore the time before which major new interventions will be required, are an important aspect of adaptation plans (for example, ref. [41]). Additionally, our framework makes projections of extreme sea levels more interpretable to policy makers, adaptation planners and the general public. While we have demonstrated the timing of 10- and 100-fold decreases, the decreases in the degree of protection that are relevant depend on the local consequences and the risk aversion[42] of practitioners. Unacceptable decreases in the degree of protection could be derived from the associated local increases in absolute risk and cost–benefit analysis (for example, refs. [21,41,43,44])— relevant considerations for both up-front and incremental adaptation strategies[45]. The risks are also governed by the mode of flooding, which

depends on the type of extreme event. As argued in ref. [14], an AF only reflects the increasing probability of a given return height, while a different type of extreme event with a different impact may become the dominant cause of that return height in the future.

Our framework can also be applied to the closure frequency of storm surge barriers (for example, refs. [15,46,47] and Fig. 6e,f), for which problematic amplifications can be derived from mechanical constraints or negative impacts on the hinterland. Additionally, it may be relevant for decision makers to consider the frequency amplification of specific flood events known to be damaging currently[14], whose return frequency may be derived from observations (for example, ref. [48]). Hence, diversifying the benchmark frequencies of AFs would aid adaptation planning, especially since the choice of benchmark affects the resulting projections (Extended Data Figs. 2, 3 and 7). In this context, improved global information on local coastal protection is needed, as systematic empirical evidence is currently lacking[32]. Although validated for several regions, the estimated flood protection standards that we used as a benchmark[21] may differ from the actual degree of local flood protection[49].

When applied locally, our timing framework could be expanded to include more granular information on hazards, vulnerability and impacts, if available. Examples are changes and variability in the seasonal sea-level cycle[50,51] and in storminess and tidal range[2,3,52–54], the effect of waves, which when included may postpone the timing of AFs[19], and the compounding effects of river discharge[55,56] and heavy rainfall[57], as well as the status of existing infrastructure, socioeconomic development[16,21] and adaptive capacity. The influence of including such aspects on adaptation planning needs a more detailed analysis. The resolution of our projections may be increased by deriving the distribution of

extreme sea levels from hydrodynamic model output (for example, refs. [2,4,58]) at locations without tide gauges. Other impacts of SLR, such as increases in the frequency and duration of high-tide flooding[20,59] and groundwater inundation[60], were not considered here but may provide additional incentive for adaptation.

The planning and implementation of large adaptation measures such as storm surge barriers or relocation can take several years to decades[15,18,22,61,62]. Our central timing estimates indicate that within the next 30 years, a 10-fold decrease in the degree of protection will occur at 26% (under SSP1-2.6) to 32% (under SSP3-7.0) of all tide gauges and a 100-fold decrease at 2% to 3%, respectively (Fig. 4). Additionally, at 4% to 8% of all tide gauges, the estimated protection standard is projected to be exceeded annually within that time (central estimates) under SSP1-2.6 and SSP3-7.0, respectively, and at 34% to 37% of all tide gauges with at least a 5% probability (Fig. 5). Even though these results are based on estimated degrees of protection, they highlight that at several locations substantial decreases in protection may occur before large adaptation measures can be completed, unless such measures can be planned and implemented faster than in the past. Our results also reveal differences in the projected timing of decreasing protection between locations that could be used by national or global investors and evaluators to compare the relative vulnerability of cities, prioritize international adaptation support and track the impacts of climate change on urban infrastructure.

Under higher emissions scenarios in which local SLR is projected to accelerate, the degree of coastal protection will decrease substantially faster in the future than it does currently (Fig. 6b). Crucially, this means that coastal adaptation planners need to consider that the available lead time and useful life time of their interventions could decrease in the future. Faster or larger adaptation increments that may require different adaptation measures would then be needed, which underlines the importance of dynamic adaptation strategies[15,18,63,64] that can be adjusted to uncertain changes in the rate of SLR. Our framework, which is premised on relating AFs to locally meaningful benchmark frequencies and projecting their timing rather than their magnitude, can help decision makers to plan both when and how to adapt within such an adaptation strategy.

Online content

Any methods, additional references, Nature Portfolio reporting summaries, source data, extended data, supplementary information, acknowledgements, peer review information; details of author contributions and competing interests; and statements of data and code availability are available at https://doi.org/10.1038/s41558-023-01616-5.

References

1. Oppenheimer, M. et al. in *IPCC Special Report on the Ocean and Cryosphere in a Changing Climate* (eds Pörtner, H.-O. et al.) Ch. 4 (IPCC, Cambridge Univ. Press, 2019).
2. Vousdoukas, M. I. et al. Global probabilistic projections of extreme sea levels show intensification of coastal flood hazard. *Nat. Commun.* **9**, 2360 (2018).
3. Howard, T., Palmer, M. D. & Bricheno, L. M. Contributions to 21st century projections of extreme sea-level change around the UK. *Environ. Res. Lett.* **1**, 095002 (2019).
4. Muis, S. et al. A high-resolution global dataset of extreme sea levels, tides, and storm surges, including future projections. *Front. Mar. Sci.* **7**, 263 (2020).
5. Hunter, J. A simple technique for estimating an allowance for uncertain sea-level rise. *Clim. Change* **113**, 239–252 (2012).
6. Church, J. A. et al. in *Climate Change 2013: The Physical Science Basis* (eds Stocker, T. F. et al.) Ch. 13 (IPCC, Cambridge Univ. Press, 2013).
7. Buchanan, M. K., Kopp, R. E., Oppenheimer, M. & Tebaldi, C. Allowances for evolving coastal flood risk under uncertain local sea-level rise. *Clim. Change* **137**, 347–362 (2016).
8. Wahl, T. et al. Understanding extreme sea levels for broad-scale coastal impact and adaptation analysis. *Nat. Commun.* **8**, 16075 (2017).
9. Frederikse, T. et al. Antarctic ice sheet and emission scenario controls on 21st-century extreme sea-level changes. *Nat. Commun.* **11**, 390 (2020).
10. Taherkhani, M. et al. Sea-level rise exponentially increases coastal flood frequency. *Sci. Rep.* **10**, 6466 (2020).
11. Fox-Kemper, B. et al. in *Climate Change 2021: The Physical Science Basis* (eds Masson-Delmotte, V. et al.) Ch. 9 (IPCC, Cambridge Univ. Press, 2021).
12. Rasmussen, D. et al. Extreme sea level implications of 1.5 °C, 2.0 °C, and 2.5 °C temperature stabilization targets in the 21st and 22nd centuries. *Environ. Res. Lett.* **13**, 034040 (2018).
13. Tebaldi, C. et al. Extreme sea levels at different global warming levels. *Nat. Clim. Change* **11**, 746–751 (2021).
14. Rasmussen, D. J., Kulp, S., Kopp, R. E., Oppenheimer, M. & Strauss, B. H. Popular extreme sea level metrics can better communicate impacts. *Clim. Change* **170**, 30 (2022).
15. Haasnoot, M. et al. Adaptation to uncertain sea-level rise; how uncertainty in antarctic mass-loss impacts the coastal adaptation strategy of the Netherlands. *Environ. Res. Lett.* **15**, 034007 (2019).
16. Haasnoot, M. et al. Long-term sea-level rise necessitates a commitment to adaptation: a first order assessment. *Clim. Risk Manag.* **34**, 100355 (2021).
17. Slangen, A. B., Haasnoot, M. & Winter, G. Rethinking sea-level projections using families and timing differences. *Earth's Future* **10**, e2021EF002576 (2022).
18. Cooley, S. et al. in *Climate Change 2022: Impacts, Adaptation and Vulnerability* (eds Pörtner H.-O. et al.) Ch. 3 (IPCC, Cambridge Univ. Press, 2022).
19. Lambert, E., Rohmer, J., Cozannet, G. L. & van de Wal, R. S. W. Adaptation time to magnified flood hazards underestimated when derived from tide gauge records. *Environ. Res. Lett.* **15**, 074015 (2020).
20. Sweet, W. et al. *Global and regional sea level rise scenarios for the United States: updated mean projections and extreme water level probabilities along U.S. coastlines*. Technical Report (NOAA, 2022).
21. Tiggeloven, T. et al. Global-scale benefit-cost analysis of coastal flood adaptation to different flood risk drivers using structural measures. *Nat. Hazards Earth Syst. Sci.* **20**, 1025–1044 (2020).
22. Mooyaart, L. F. & Jonkman, S. N. Overview and design considerations of storm surge barriers. *J. Waterw. Port, Coast. Ocean Eng.* https://doi.org/10.1061/(asce)ww.1943-5460.0000383 (2017).
23. Reeder, T. & Ranger, N. *How Do You Adapt in an Uncertain World? Lessons from the Thames Estuary 2100 Project* (World Resources Report, 2011).
24. Kwadijk, J. C. et al. Using adaptation tipping points to prepare for climate change and sea level rise: a case study in the Netherlands. *Wiley Interdiscip Rev. Clim. Change* **1**, 729–740 (2010).
25. Haasnoot, M., Middelkoop, H., Offermans, A., van Beek, E. & van Deursen, W. P. Exploring pathways for sustainable water management in river deltas in a changing environment. *Clim. Change* **115**, 795–819 (2012).
26. Garner, G. et al. IPCC AR6 sea level projections. *Zenodo* https://doi.org/10.5281/zenodo.6382554 (2021).
27. Meinshausen, M. et al. The shared socio-economic pathway (SSP) greenhouse gas concentrations and their extensions to 2500. *Geosci. Model Dev.* **13**, 3571–3605 (2020).
28. Solari, S., Egüen, M., Polo, M. J. & Losada, M. A. Peaks over threshold (POT): a methodology for automatic threshold estimation using goodness of fit p-value. *Water Resour. Res.* **53**, 2833–2849 (2017).

29. Haigh, D. et al. GESLA Version 3: a major update to the global higher-frequency sea-level dataset. *Geosci. Data J.* **00**, 1–22 (2022).

30. Woodworth, P. L. et al. Towards a global higher-frequency sea level data set. *Geosci. Data J.* **3**, 50–59 (2017).

31. Scussolini, P. et al. FLOPROS: an evolving global database of flood protection standards. *Nat. Hazards Earth Syst. Sci.* **16**, 1049–1061 (2016).

32. Hinkel, J. et al. Uncertainty and bias in global to regional scale assessments of current and future coastal flood risk. *Earth's Future* **9**, e2020EF001882 (2021).

33. Vitousek, S. et al. Doubling of coastal flooding frequency within decades due to sea-level rise. *Sci. Rep.* **7**, 1399 (2017).

34. Bloemendaal, N. et al. Generation of a global synthetic tropical cyclone hazard dataset using storm. *Sci. Data* **7**, 40 (2020).

35. Dullaart, J. C. M. et al. Accounting for tropical cyclones more than doubles the global population exposed to low-probability coastal flooding. *Commun. Earth Environ.* https://doi.org/10.1038/s43247-021-00204-9 (2021).

36. Haigh, I. D. et al. Estimating present day extreme water level exceedance probabilities around the coastline of Australia: tropical cyclone-induced storm surges. *Clim. Dyn.* **42**, 139–157 (2014).

37. O'Grady, J. G., Stephenson, A. G. & McInnes, K. L. Gauging mixed climate extreme value distributions in tropical cyclone regions. *Sci. Rep.* **12**, 4626 (2022).

38. *Thames Estuary 2100 (TE2100)*. Technical Report (Environment Agency, 2012).

39. Fang, J. et al. Coastal flood risks in China through the 21st century - an application of DIVA. *Sci. Total Environ.* **704**, 135311 (2020).

40. Brink, H. W. V. D. & Goederen, S. D. Recurrence intervals for the closure of the Dutch Maeslant surge barrier. *Ocean Sci.* **13**, 691–701 (2017).

41. Penning-Rowsell, E. C., Haigh, N., Lavery, S. & McFadden, L. A threatened world city: the benefits of protecting London from the sea. *Nat. Hazards* **66**, 1383–1404 (2013).

42. Hinkel, J. et al. Meeting user needs for sea level rise information: a decision analysis perspective. *Earth's Future* **7**, 320–337 (2019).

43. Rasmussen, D. J., Buchanan, M. K., Kopp, R. E. & Oppenheimer, M. A flood damage allowance framework for coastal protection with deep uncertainty in sea level rise. *Earth's Future* **8**, e2019EF001340 (2020).

44. Eijgenraam, C. et al. Economically efficient standards to protect the Netherlands against flooding. *Interfaces* **44**, 7–21 (2014).

45. Hall, J. W., Brown, S., Nicholls, R. J., Pidgeon, N. F. & Watson, R. T. Proportionate adaptation. *Nat. Clim. Change* **2**, 833–834 (2012).

46. Lionello, P., Nicholls, R. J., Umgiesser, G. & Zanchettin, D. Venice flooding and sea level: past evolution, present issues, and future projections (introduction to the special issue). *Nat. Hazards Earth Syst. Sci.* **21**, 2633–2641 (2021).

47. Hall, J. W., Harvey, H. & Manning, L. J. Adaptation thresholds and pathways for tidal flood risk management in london. *Clim. Risk Manag.* **24**, 42–58 (2019).

48. Idier, D. et al. Coastal flood: a composite method for past events characterisation providing insights in past, present and future hazards-joining historical, statistical and modelling approaches. *Nat. Hazards* **101**, 465–501 (2020).

49. Hallegatte, S., Green, C., Nicholls, R. J. & Corfee-Morlot, J. Future flood losses in major coastal cities. *Nat. Clim. Change* **3**, 802–806 (2013).

50. Widlansky, M. J., Long, X. & Schloesser, F. Increase in sea level variability with ocean warming associated with the nonlinear thermal expansion of seawater. *Commun. Earth Environ.* **1**, 9 (2020).

51. Hermans, T. H. J. et al. The effect of wind stress on seasonal sea-level change on the Northwestern European Shelf. *J. Clim.* **35**, 1745–1759 (2021).

52. Pickering, M. D. et al. The impact of future sea-level rise on the global tides. *Continental Shelf Res.* **142**, 50–68 (2017).

53. Haigh, I. D. et al. The tides they are a changin': a comprehensive review of past and future non astronomical changes in tides, their driving mechanisms and future implications. *Rev. Geophysics* **57**, 2018RG000636 (2019).

54. Rashid, M. M., Wahl, T. & Chambers, D. P. Extreme sea level variability dominates coastal flood risk changes at decadal time scales. *Environ. Res. Lett.* **16**, 024026 (2021).

55. Ward, P. J. et al. Dependence between high sea-level and high river discharge increases flood hazard in global deltas and estuaries. *Environ. Res. Lett.* **13**, 084012 (2018).

56. Couasnon, A. et al. Measuring compound flood potential from river discharge and storm surge extremes at the global scale and its implications for flood hazard. *Nat. Hazards Earth Syst. Sci.* **20**, 489–504 (2019).

57. Wahl, T. & Chambers, D. P. Evidence for multidecadal variability in US extreme sea level records. *J. Geophys. Res. Oceans* **120**, 1527–1544 (2015).

58. Kirezci, E. et al. Projections of global-scale extreme sea levels and resulting episodic coastal flooding over the 21st century. *Sci. Rep.* **10**, 11629 (2020).

59. Thompson, P. R. et al. Rapid increases and extreme months in projections of United States high-tide flooding. *Nat. Clim. Change* **11**, 584–590 (2021).

60. Rotzoll, K. & Fletcher, C. H. Assessment of groundwater inundation as a consequence of sea-level rise. *Nat. Clim. Change* **3**, 477–481 (2013).

61. Hallegatte, S. Strategies to adapt to an uncertain climate change. *Glob. Environ. Change* **19**, 240–247 (2009).

62. Rasmussen, D. J., Kopp, R. E., Shwom, R. & Oppenheimer, M. The political complexity of coastal flood risk reduction: lessons for climate adaptation public works in the U.S. *Earth's Future* **9**, e2020EF001575 (2021).

63. Haasnoot, M., Kwakkel, J. H., Walker, W. E. & ter Maat, J. Dynamic adaptive policy pathways: a method for crafting robust decisions for a deeply uncertain world. *Glob. Environ. Change* **23**, 485–498 (2013).

64. Barnett, J. et al. A local coastal adaptation pathway. *Nat. Clim. Change* **4**, 1103–1108 (2014).

Methods

We compute probabilistic projections of the timing of the frequency AFs of extreme sea levels due to SLR, relative to estimated flood protection standards[21] and using high-frequency tide gauge observations from GESLA3[29] and relative sea-level projections from IPCC AR6[11]. In this section, we describe the steps taken to analyse the GESLA3 data, to compute the SLR required for a range of AFs and to project when those AFs will occur (see Extended Data Fig. 9 for a flowchart).

Processing GESLA3 data

We analyse observed extreme sea levels using high-frequency coastal tide gauge records from GESLA3 without identified data issues[29]. Daily maxima (composed of tides and surges) are derived from hourly-mean data for days with at least 12 hourly means available, following ref. [12]. We only consider tide gauges providing at least 30 years worth of daily maxima. If multiple records are available for the same location, or for locations less than 3 km apart, we use the longest record. This procedure leaves 523 records for further analysis, of which approximately 50% provide more than 49 years worth of daily maxima and 25% more than 58 years. As our statistical analysis requires independent and identically distributed observations, we detrend the daily maxima by subtracting a linear fit and subsequently subtract the mean seasonal cycle. To ensure independence, we additionally decluster the events higher than the 95th percentile with a commonly used 3-day moving window[65].

Modelling extreme sea levels

Following previous studies[7–9,11,12,14], we model extreme sea levels using a peak-over-threshold method and fitting a generalized Pareto distribution to the observed peaks. Unlike most of these studies (with the exception of ref. [19]), we do not use a fixed threshold percentile above which we characterize daily maxima as extreme, but determine the threshold for each tide gauge individually using an automatic threshold selection method (see ref. [28] for details). The selection method fits generalized Pareto distributions to the declustered daily maxima above a range of thresholds, using each declustered value higher than the 95th percentile as a potential threshold. The threshold that minimizes the complement of the P value of the Anderson–Darling goodness-of-fit test is selected. The method tends to yield similar thresholds as selection by visual inspection of parameter instability[28]. The median threshold percentile selected at the GESLA3 tide gauges is approximately 98.8% and the median annual exceedance rate is approximately three events per year.

Computing return curves based on distribution parameters

The generalized Pareto distribution is specified by the location parameter μ (the selected threshold), the scale parameter σ and the shape parameter ξ (ref. [66]). Central estimates of the σ and ξ parameters are determined by applying maximum likelihood estimation to all declustered peaks above the selected threshold μ. The confidence intervals of σ and ξ are estimated through bootstrapping[28]. Knowing μ, σ and ξ, the probability of y is given by[66]:

$$F(y) = \begin{cases} 1 - (1 + \xi y/\sigma)^{-1/\xi}, & \text{for } \xi \neq 0 \\ 1 - e^{-y/\sigma}, & \text{for } \xi = 0 \end{cases} \quad (1)$$

with $y = z - \mu$ the return height z relative to μ, defined on $\{y: y > 0$ and $(1 + \xi y/\sigma) > 0\}$. If the shape parameter ξ is negative, the distribution has an upper bound of $y = -\sigma/\xi$, if is positive, the distribution is unbounded, and if $\xi = 0$ the distribution is exponential (log-linear).

Assuming the probability of $z > \mu$ is Poisson-distributed, the expected number of annual exceedances of z follows from:

$$N(z) = \begin{cases} \lambda(1 + \xi(z-\mu)/\sigma)^{-1/\xi}, & \text{for } \xi \neq 0 \\ \lambda e(-(z-\mu)/\sigma), & \text{for } \xi = 0 \end{cases} \quad (2)$$

where λ is the average expected number of annual exceedances of threshold μ. By rearranging equation (2), the height z can be solved for a given annual exceedance probability $N(z)$:

$$z = \begin{cases} \sigma/\xi((N(z)/\lambda)^{\xi/-1} - 1) + \mu, & \text{for } \xi \neq 0 \\ -\sigma\ln(N(z)/\lambda) + \mu, & \text{for } \xi = 0 \end{cases} \quad (3)$$

We use equation (3) to model the return curves for a range of input return frequencies. We obtain the central-estimate return curve by inserting the central-estimate σ and ξ parameters into equation (3). Additionally, we obtain 10,000 return curve samples by inserting the same number of samples of σ and ξ drawn from their estimated confidence intervals, following refs. [1,11,33].

Modelling sea levels below the generalized Pareto distribution

In some instances, we wish to evaluate AFs to a frequency higher than the average annual exceedance (λ) of the selected threshold (μ), that is, below the support of the generalized Pareto distribution. For that, the bulk data below the threshold needs to be characterized. Following ref. [20], we do so by estimating the return heights with a return frequency higher than λ yr^{-1} by logarithmically extrapolating the return heights with a return frequency between 0.5 yr^{-1} and λ yr^{-1}, up to a return frequency of 10 yr^{-1}. For a few edge cases, $\lambda < 0.5$ yr^{-1} and we extrapolate using 0.2 yr^{-1} as the lower boundary. This is similar to applying a Gumbel distribution to model the bulk data between μ and mean higher high water[7,11,12]. We note that such extrapolations are limited characterizations of the observations, but the extent to which declustering the bulk data is appropriate for alternatives such as extreme value mixture models[14,67] and the empirical distribution is not yet clear. Our method allows us to evaluate AFs of 100 relative to degrees of protection down to 0.1 yr^{-1}. At all the GESLA3 tide gauges that we consider, the estimated flood protection standards of ref. [21] (see next paragraph) are associated with return frequencies lower than 0.1 yr^{-1}.

Computing required SLR

To project the timing of AFs, we use the concept of required SLR (Fig. 2a). Required SLR refers to the SLR required to establish a given amplification of a reference return frequency f_{Ref}. The required SLR is derived from a return curve in two steps. First, the return height corresponding to f_{Ref} is subtracted from the return curve. Second, the referenced return curve is inverted. Hence, the required SLR indicates the vertical translation of the return curve required to establish a certain horizontal translation in a height-frequency graph relative to f_{Ref} (Fig. 2a). The required SLR therefore depends on the form of the return curve between f_{Ref} and a new increased return frequency[10,33], with the form of the return curve determined by the σ and ξ parameters (schematically shown in Extended Data Fig. 2). Like previous studies[1,7,9,11–14], we assume that σ and ξ are time-constant and do not consider dynamic changes in tides, storm surges and waves, and their interaction. At many locations, this is a reasonable assumption because SLR is the dominant driver of changes in extreme sea levels compared to dynamic changes in tides and surges[2,4]. Additionally, projections of dynamic changes in tides and surges are still hampered by limited model fidelity, small ensemble sizes and the low resolution of the global climate models from which changes in atmospheric forcing are typically derived, and are not provided as continuous time series up to 2150, which we need for our analysis. From the central-estimate return curve and the 10,000 sample return curves (see previous paragraph), the central estimate of the required SLR curve as well as 10,000 required SLR curve samples are obtained, respectively. The percentiles presented in the paper (Fig. 3c,d,e,f) reflect the distribution of these samples.

Using estimated flood protection standards

By setting f_{Ref} to the return frequency corresponding with the degree of local coastal flood protection instead of to an arbitrary benchmark

frequency such as 0.01 yr⁻¹, local context can be added to AFs. Systematic global information on the local degree of coastal flood protection is, however, not yet available[32]. For our global-scale analysis, we therefore base f_{Ref} on estimates of local flood protection standards ($f_{FLOPROS}$ (ref. [21])), as in ref. [16]. We assign the estimated flood protection standards, which range from 0.5 to 0.001 yr⁻¹, to the GESLA3 tide gauges according to their nearest subnational unit ($f_{Ref} = f_{FLOPROS}$; Fig. 2b). For the subnational units nearest to 46 tide gauges, no FLOPROS estimates are available, either because no inundation was simulated or because of a lack of underlying exposure data (for instance, at small islands in the Pacific and Indian Ocean)[21]. We therefore exclude these tide gauges from our analysis, leaving a total of 477 tide gauges.

To show the influence of using a locally varying $f_{Ref} = f_{FLOPROS}$, we also compare our results to using $f_{Ref} = 0.01$ yr⁻¹ at all locations, that is, the benchmark return frequency often used for AFs. In Fig. 6, in which we illustrate how our projections can be used for three coastal cities, we base f_{Ref} on real-world examples.

Projecting the timing of AFs

Having estimated the SLR required for AFs relative to f_{Ref}, the timing of the AFs can be projected by combining the required SLR with projected relative SLR at each location. We use the relative sea-level projections of the IPCC AR6 (ref. [11,26]) nearest to the GESLA3 tide gauges, for SSP scenarios[27] SSP1-2.6, SSP2-4.5, SSP3-7.0 and SSP5-8.5. Sea-level projections were not available for three tide gauges, so we dropped these. The projections of IPCC AR6 are based on probability boxes[68] that encompass the cumulative distribution functions of the SLR projected using different workflows (see Table 9.7 of ref. [11]). To project the timing of the AFs, for each scenario we use the two medium confidence workflows that extend to 2150. This ensures that the results are continuous across 2100, which is the year in which the other medium confidence workflows of IPCC AR6 end. Separately for SSP1-2.6 and SSP5-8.5, we also incorporate the two low confidences workflows, labelling the outcomes with 'SSP1-2.6-lowconf' and 'SSP5-8.5-lowconf'.

To retain the correlation structure of the SLR projections, for each considered workflow and scenario we use the raw projection samples available at https://github.com/Rutgers-ESSP/IPCC-AR6-Sea-Level-Projections. The time series samples are provided as 19-year averages at decadal intervals from 2020 to 2150, relative to the mean sea level during the period 1995–2014. For each sample, we obtain projections for intermediate years through quadratic interpolation and reference the resulting time series to either 2022 (present-day) or a future year to demonstrate the influence of the projected changes in the rate of SLR on the timing of AFs (Fig. 5). While the annual SLR values derived do not account for interannual sea-level variability, interannual sea-level variability is retained in the GESLA3 observations. To project the timing of AFs, we interpolate the timing of the projected SLR onto the SLR required for the AFs.

To compute the central-estimate timing of the AFs, we combine the central estimate of required SLR with the median projected SLR of the probability box bounding the distributions of the considered workflows, for each scenario. Consistent with the SLR projections used, we compute the distribution of the projected timing as the probability box bounding the distributions of the projected timing for the workflows considered, for each scenario. To compute the distribution for each considered workflow, we randomly combine the 10,000 samples of required SLR with 10,000 of the raw samples of projected SLR. From the resulting 10,000 timing samples for each workflow, the distributions of the projected timing of the AFs are derived. As we use SLR projections until 2150, the timing of the AFs cannot be evaluated for all samples at all locations. For instance, slow positive SLR may evaluate to a timing beyond 2150, and a relative sea-level fall will lead to a decrease in return frequency. If, as a

result, central estimates or the percentiles of the probability boxes presented evaluate to later than 2150 or to never, we display no value (for example, white and cyan in Fig. 3, respectively). For the same reason, the median of a probability box, which is the mean of the medians of the distributions bounded by that box, cannot be determined if the median timing for one workflow evaluates to beyond 2150 while for the other it is earlier than 2150. Therefore, the medians of the probability boxes are not computed.

References

65. Haigh, I. D. et al. Spatial and temporal analysis of extreme sea level and storm surge events around the coastline of the UK. *Sci. Data* **3**, 160107 (2016).
66. Coles, S. *An Introduction to Statistical Modeling of Extreme Values* (Springer, 2001).
67. Ghanbari, M., Arabi, M., Obeysekera, J. & Sweet, W. A coherent statistical model for coastal flood frequency analysis under nonstationary sea level conditions. *Earth's Future* **7**, 162–177 (2019).
68. Cozannet, G. L., Manceau, J. & Rohmer, J. Bounding sea level projections within the framework of the possibility theory. *Environ. Res. Lett.* **12**, 014012 (2017).
69. Hermans, T. H. J. et al. Projections of the timing of decreasing coastal flood protection. *Zenodo* https://doi.org/10.5281/zenodo.7505441 (2023).
70. Hermans, T. H. J. & Malagon-Santos, V. Timingafs: v1.0.0. *Zenodo* https://doi.org/10.5281/zenodo.7503089 (2023).
71. Jane, R., Cadavid, L., Obeysekera, J. & Wahl, T. Multivariate statistical modelling of the drivers of compound flood events in south Florida. *Nat. Hazards Earth Syst. Sci.* **20**, 2681–2699 (2020).

Author contributions

T.H.J.H. conceived the study in consultation with A.B.A.S., C.A.K., R.E.K., M.O., D.J.R., M.H. and V.M.-S. T.H.J.H. produced the results and figures and led the writing of the paper, with input from all coauthors. G.G.G. provided the sea-level projections. T.H.J.H. and V.M.-S. processed the GESLA3 observations, and V.M.-S. and R.A.J. performed the automatic threshold selection.

Additional information

Extended data is available for this paper at
https://doi.org/10.1038/s41558-023-01616-5.

Correspondence and requests for materials should be addressed to
Tim H. J. Hermans.

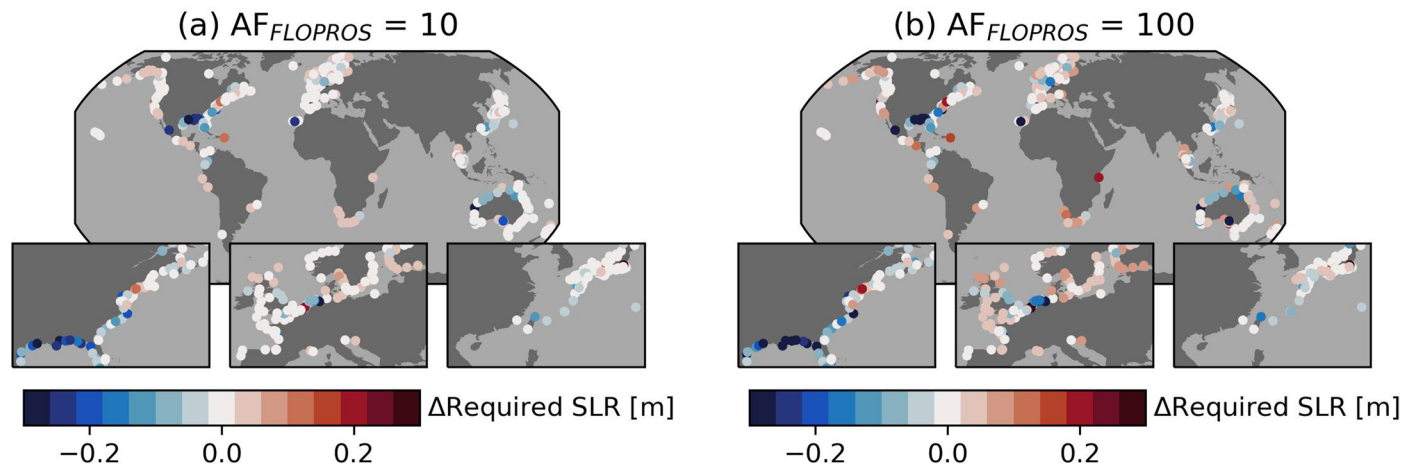**Reprints and permissions information** is available at
www.nature.com/reprints.
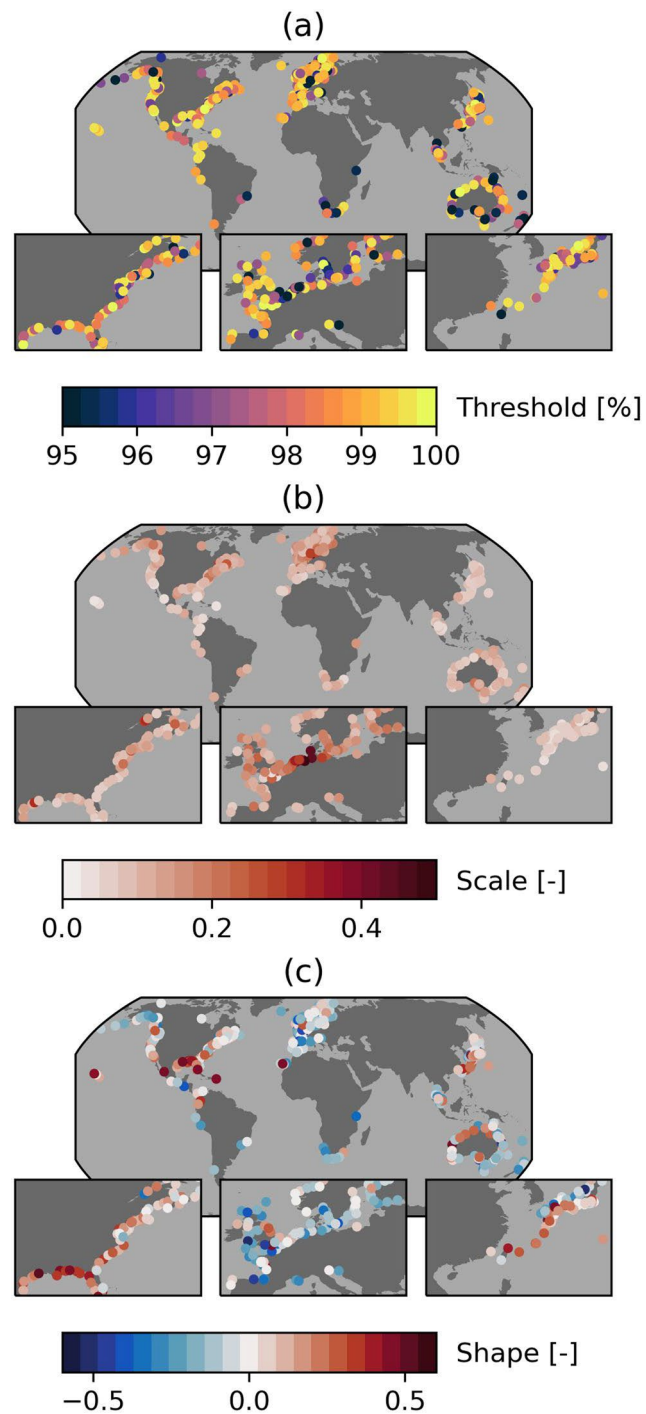
Extended Data Fig. 1 | Generalized Pareto distribution parameters. a, selected threshold percentiles, **b**, central estimate of scale parameters, **c**, central estimate of shape parameters. The map insets zoom in on three regions densely covered with tide gauges (US East Coast, Europe and Southeast Asia).
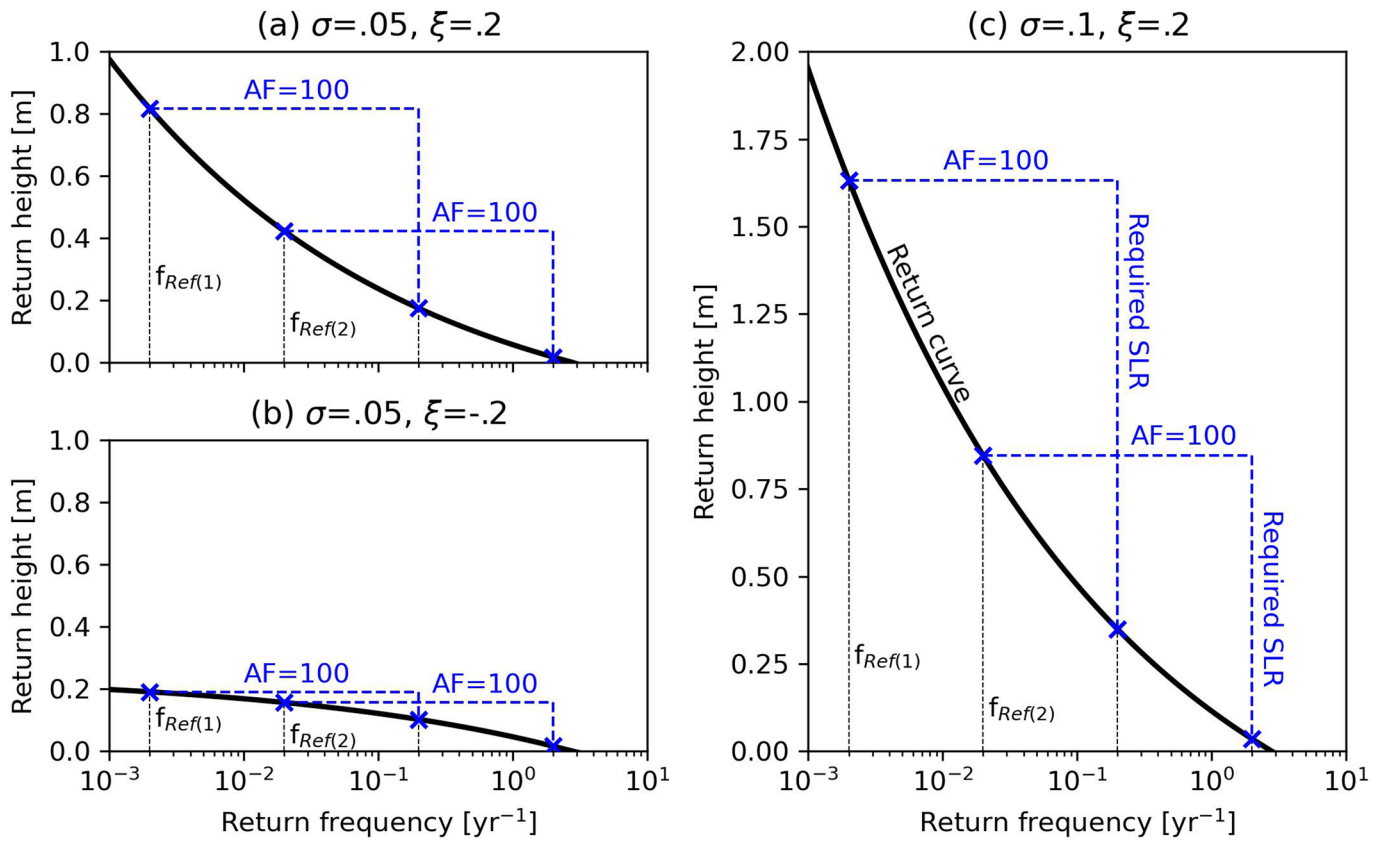
**Extended Data Fig. 2 | Schematic influence of distribution parameters and f_{Ref} on required SLR.** Schematic illustration of how the required SLR for an amplification factor of 100 (blue, vertical lines) depends on the form of the return curve (black) and on the reference return frequency f_{Ref}, for different scale (σ) and shape (ξ) parameters: **a**, $\sigma = 0.05$, $\xi = 0.2$; **b**, $\sigma = 0.05$, $\xi = -0.2$; **c**, $\sigma = 0.1$, $\xi = 0.2$. The y-axis in **c** was extended to accommodate the steep return curve and large required SLR.

(a) AF$_{FLOPROS}$ = 10

(b) AF$_{FLOPROS}$ = 100
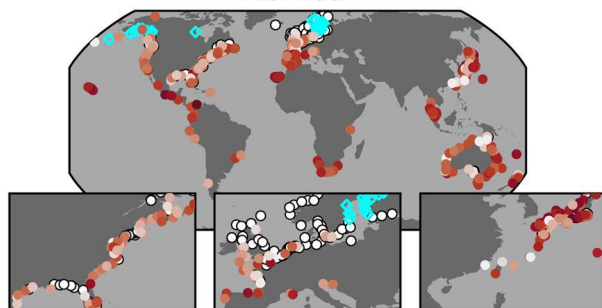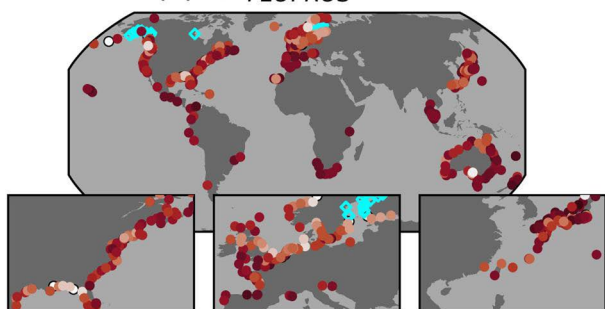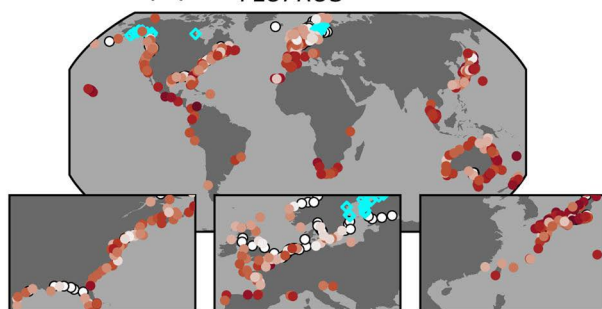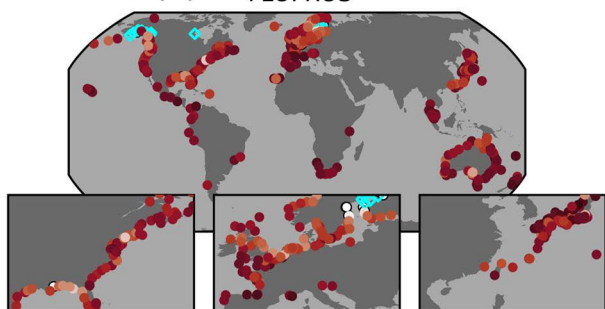
ΔRequired SLR [m]

−0.2　　0.0　　0.2

ΔRequired SLR [m]

−0.2　　0.0　　0.2

Extended Data Fig. 3 | Sensitivity of required SLR to f$_{Ref}$. a, central estimate of required SLR [m] for AF$_{FLOPROS}$ = 10 minus that for AF$_{0.01}$ = 10. **b**, central estimate of required SLR [m] for AF$_{FLOPROS}$ = 100 minus that for AF$_{0.01}$ = 100.
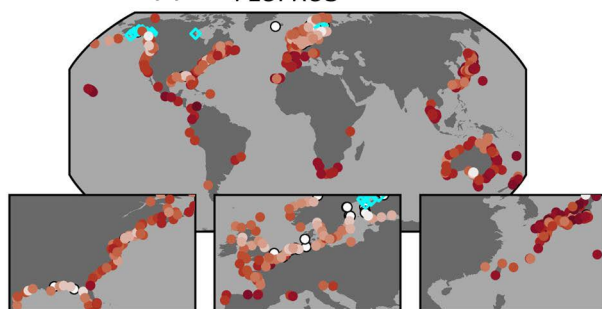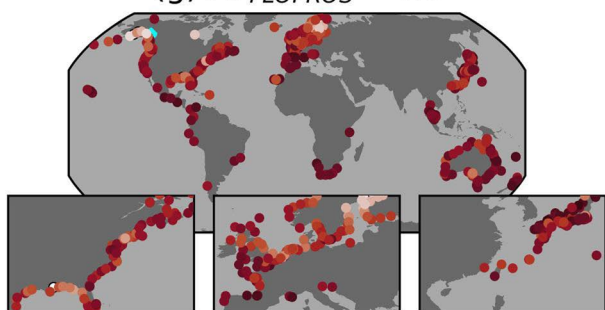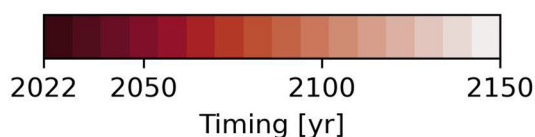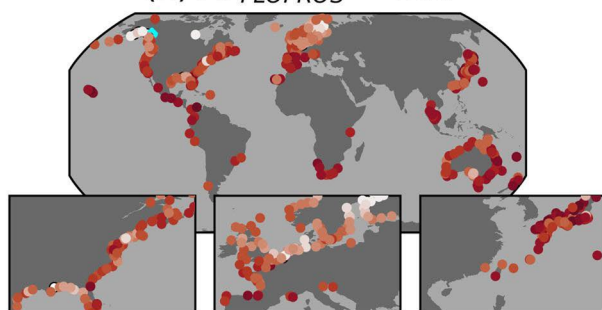
SSP1-2.6-lowconf

Extended Data Fig. 4 | Projected timing of AF$_{FLOPROS}$ = 10 and 100. a, c, e & g, central estimate of the timing [yr] of AF$_{FLOPROS}$ = 10 at GESLA3 tide gauges (SSP1-2.6-lowconf, SSP2-4.5, SSP5-8.5 & SSP5-8.5-lowconf). **b, d, f & h,** as in **a, c, e & g,** but for AF$_{FLOPROS}$ = 100. White indicates where the projected timing evaluates to later than 2150 and cyan indicates where a relative sea-level fall is projected. The map insets zoom in on three regions densely covered with tide gauges (US East Coast, Europe and Southeast Asia).
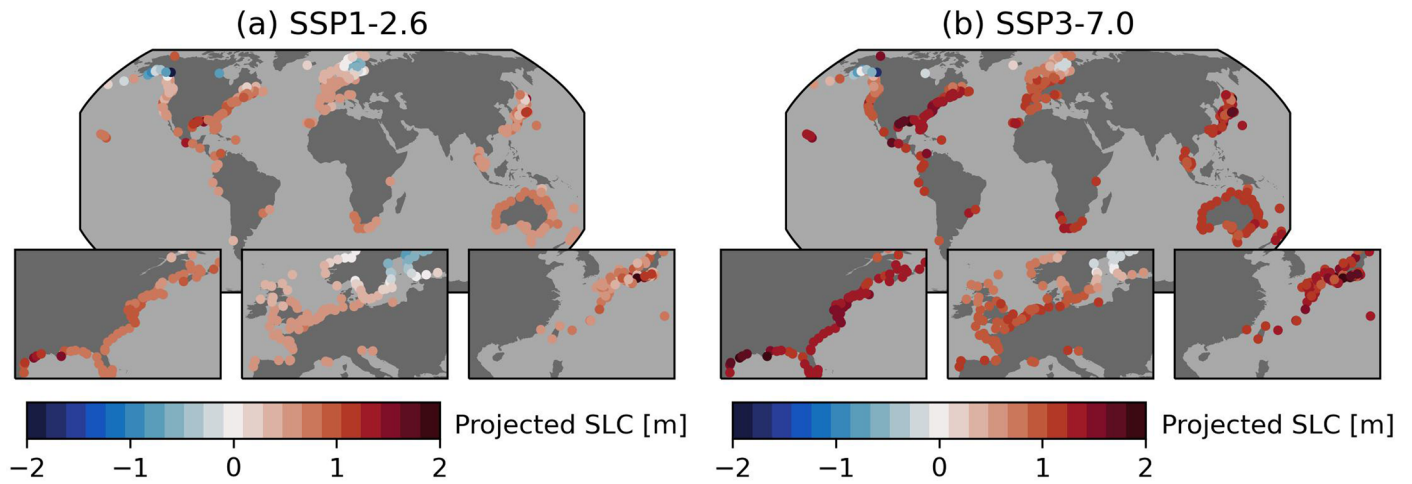
(a) SSP1-2.6

(b) SSP3-7.0

Extended Data Fig. 5 | Relative sea-level change projected for 2150.
Median sea-level projections of IPCC AR6[11,26] at GESLA3 tide gauges, in 2150 relative to 2022, for **a**, SSP1-2.6, and **b**, SSP3-7.0. The median at each location is derived from the probability box bounding the distributions of the workflows extending to 2150 (see Methods). The map insets in the other subpanels zoom in on three regions densely covered with tide gauges (US East Coast, Europe and Southeast Asia).
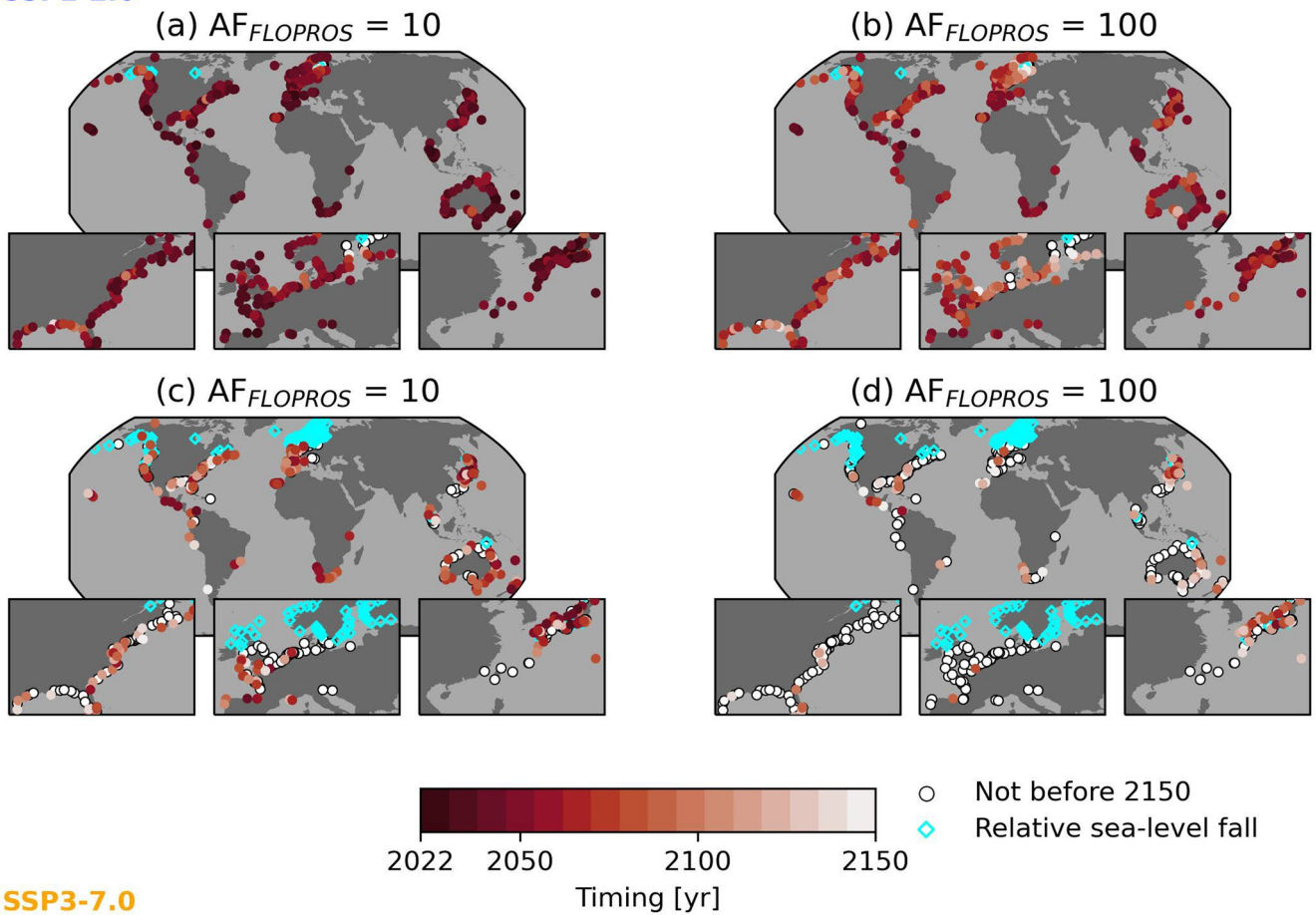
SSP1-2.6

SSP3-7.0
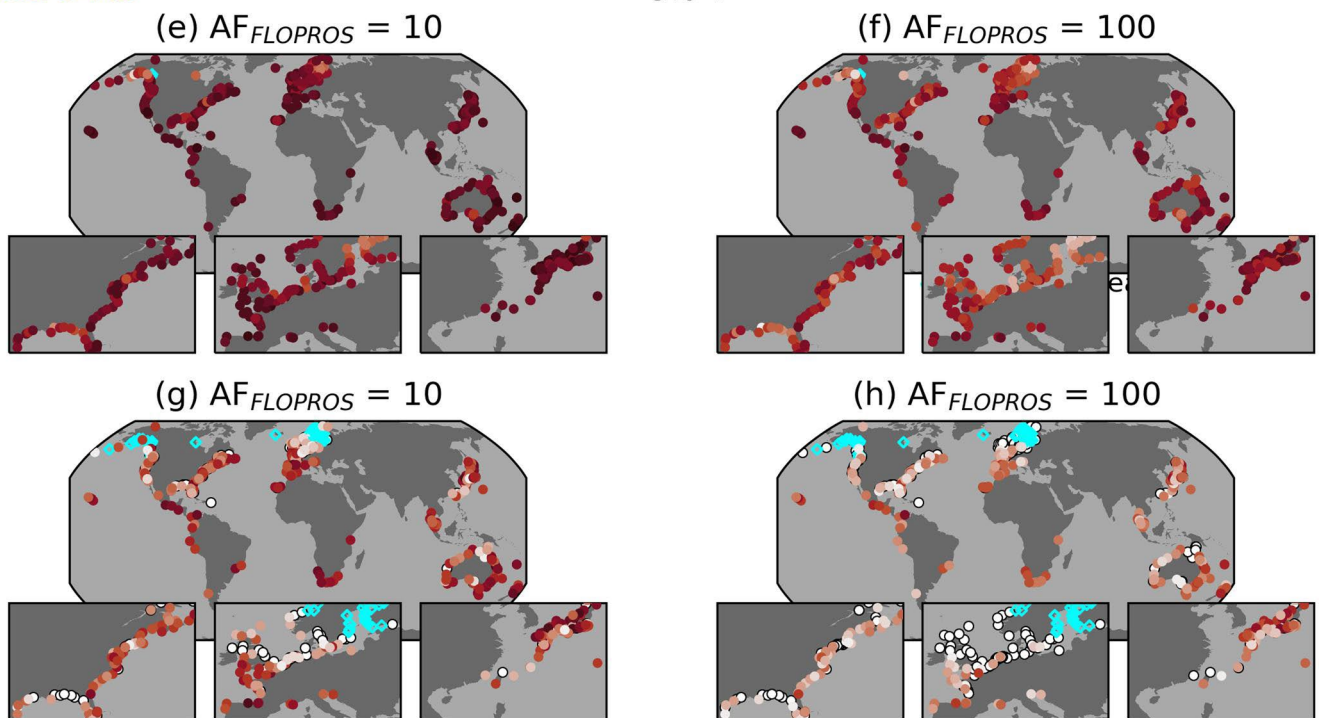
Extended Data Fig. 6 | Projected timing percentiles of AF$_{FLOPROS}$ = 10 and 100. **a, & b**, 5th and **c, & d**, 95th percentiles of the probability box of the projected timing [yr] of AF$_{FLOPROS}$ = 10 and 100 (SSP1-2.6). **e, f, g & h**, as in **a, b, c & d**, but for SSP3-7.0. White indicates where the proj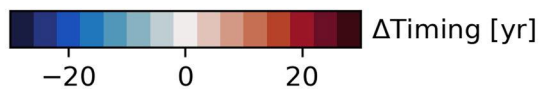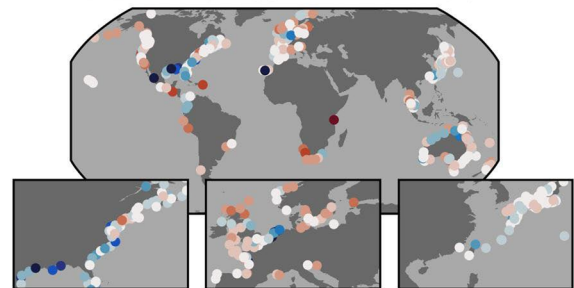ected timing evaluates to later than 2150 and cyan indicates where a relative sea-level fall is projected. The map insets zoom in on three regions densely covered with tide gauges (US East Coast, Europe and Southeast Asia).
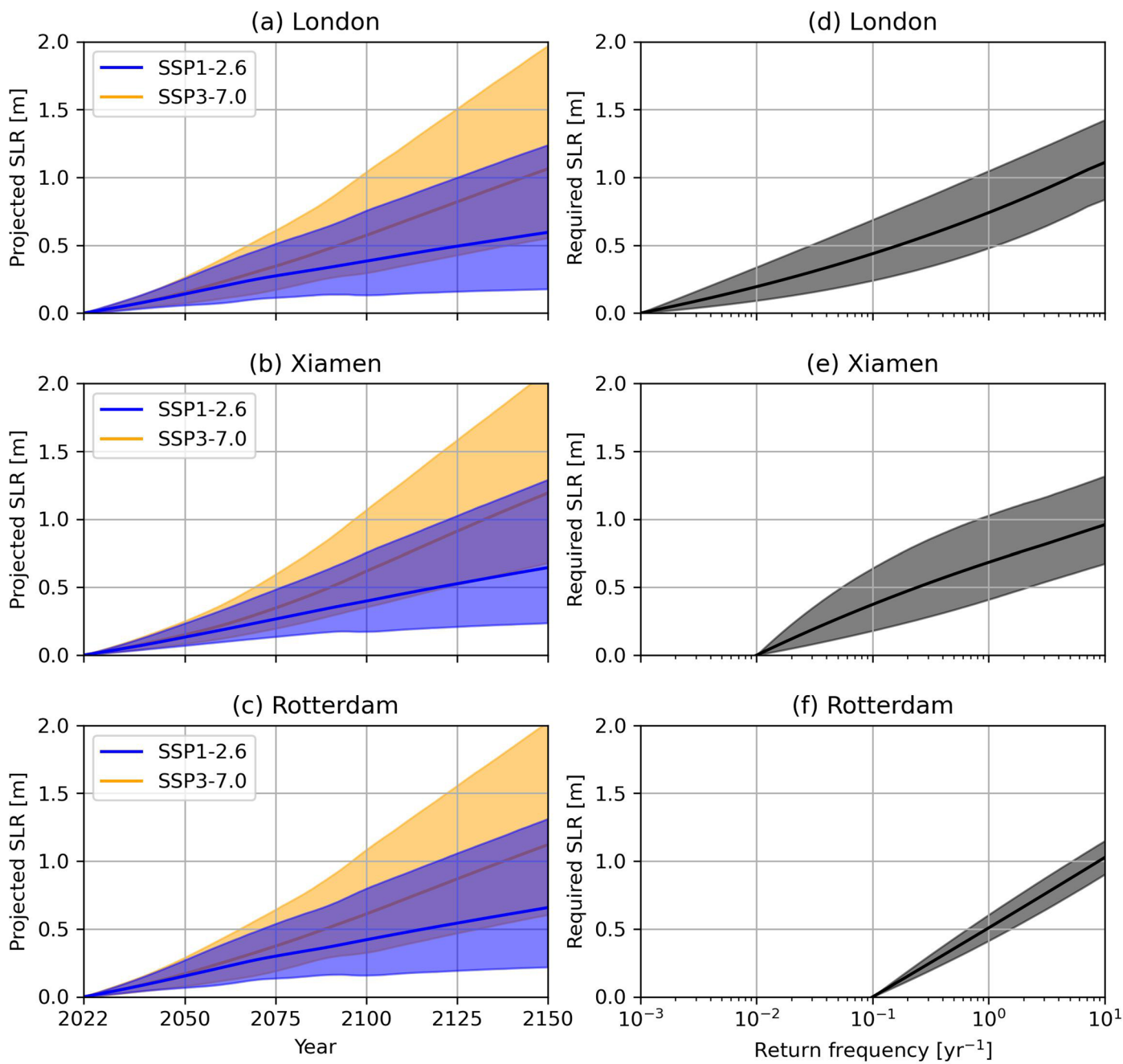
SSP1-2.6

(a) Local minus fixed threshold
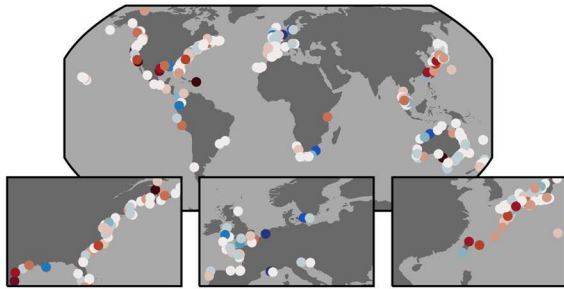
(c) AF$_{FLOPROS}$ minus AF$_{0.01}$
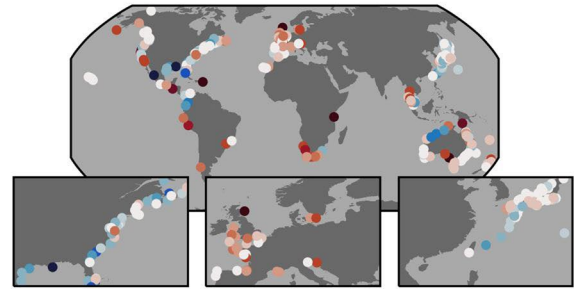
SSP3-7.0

## (b) Local minus fixed threshold
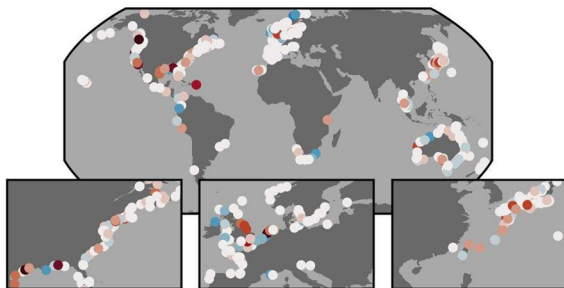
(d) AF$_{FLOPROS}$ minus AF$_{0.01}$
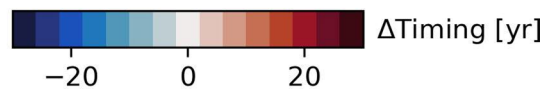
Extended Data Fig. 7 | Sensitivity of projected timing. a-b, central timing estimates of AF$_{FLOPROS}$ = 100 derived using locally selected thresholds (Extended Data Fig. 1a) minus those derived using the median selected threshold percentile 98.8% at each tide gauge [yr], under SSP1-2.6 (blue) and SSP3-7.0 (orange). **c-d**, central timing estimates of AF$_{FLOPROS}$ = 100 minus those of AF$_{0.01}$ = 100 [yr], under SSP1-2.6 (blue) and SSP3-7.0 (orange). Timing differences are only displayed where both compared estimates evaluate to before 2150. The map insets in the other subpanels zoom in on three regions densely covered with tide gauges (US East Coast, Europe and Southeast Asia).

Extended Data Fig. 8 | Projected and required SLR at three coastal cities. **a, b, & c,** projected relative SLR of IPCC AR6[11,26] nearest to tide gauges 'Sheerness', 'Xiamen' and 'Hoek_van_Holland' under SSP1-2.6 (blue) and SSP3-7.0 (orange), relative to 2022. The solid lines indicate the medians and the shading the 5-95% ranges of the probability boxes. **d, e, & f,** required SLR for the amplification of f_{Ref} (see Fig. 6) at these locations. The solid lines indicate the central estimates and the shading the 5-95% ranges. Combining the projected and required SLR samples shaping the distributions shown in this figure results in the projected timing in Fig. 6.
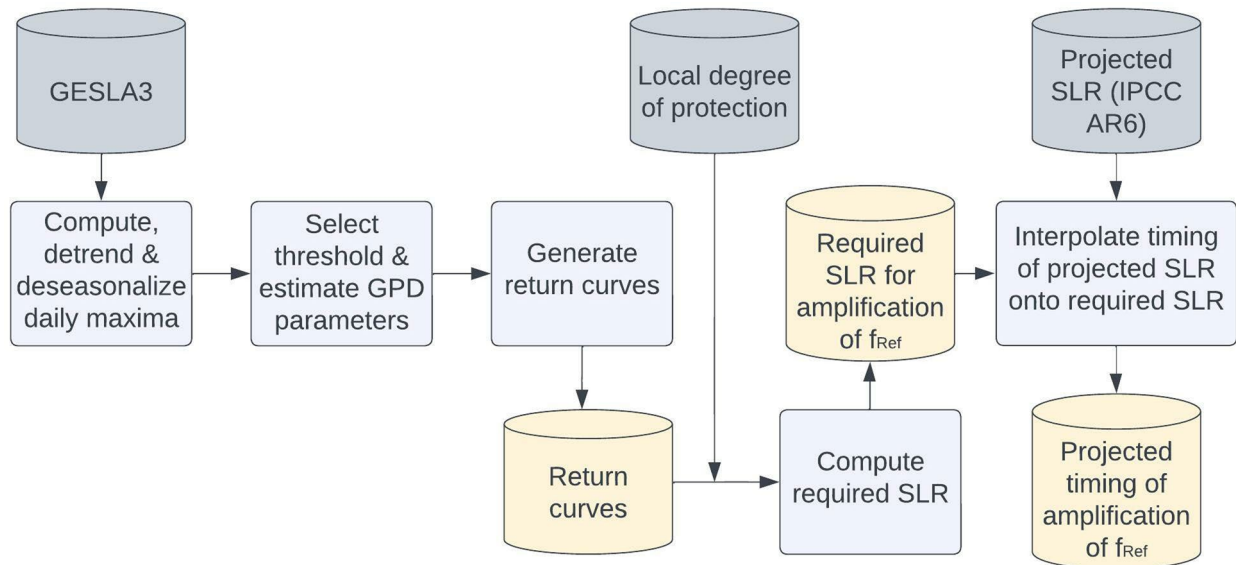
Extended Data Fig. 9 | Methodology flowchart. Methodology used to project the timing of amplification factors. Grey: input data; lightblue: steps taken; yellow: output obtained.